THE ASTROPHYSICAL JOURNAL, 491:939–951, 1997 December 20
© 1997. The American Astronomical Society. All rights reserved. Printed in U.S.A.

ELECTRON ACCELERATION IN SOLAR FLARES BY FAST MODE WAVES: QUASI-LINEAR THEORY AND PITCH-ANGLE SCATTERING

JAMES A. MILLER
Department of Physics, University of Alabama in Huntsville, Huntsville, AL 35899; miller@mpingo.uah.edu
Received 1997 June 3; accepted 1997 July 30

ABSTRACT

It has been shown recently that small-amplitude, long-wavelength, fast mode waves can accelerate a large number of electrons from the ambient thermal distribution to relativistic energies on subsecond timescales and can thereby account for the general properties of electron acceleration in impulsive solar flare energy release fragments. This prior study employed quasi-linear theory as well as the assumption that ancillary pitch-angle scattering kept the electron distribution isotropic. In light of the high efficiency of the resulting stochastic acceleration process, we question the necessity of pitch-angle scattering in the model and the validity of quasi-linear theory in describing the wave-particle interaction. We find that quasi-linear theory does predict accurately the behavior of electrons, even when the turbulence has an energy density about equal to the ambient magnetic field energy density, and that pitch-angle scattering is a necessary condition for acceleration. We also discuss the more general issue of modeling continuous wave spectra by discrete ones for use in test particle simulations.

Subject headings: acceleration of particles — plasmas — Sun: corona — Sun: flares — Sun: particle emission — waves

1. INTRODUCTION

During impulsive solar flares, large numbers of electrons are rapidly accelerated (probably in the lower corona) to relativistic energies for tens to hundreds of seconds. Some of these electrons propagate downward to the solar chromosphere and produce the hard X-ray ($\gtrsim 20$ keV) bremsstrahlung emission that is probably the most defining characteristic of such flares (see, e.g., Dennis 1985; Lin & Schwartz 1987). The energy content in electrons with energy greater than 20 keV typically exceeds 10^{31} ergs in a large flare, which corresponds to the annihilation of ≈ 500 G of magnetic field over a volume of 10^{27} cm^3. Understanding the process(es) responsible for this acceleration (see review by Miller et al. 1997) is of fundamental importance in high-energy solar physics.

Stochastic acceleration by plasma turbulence consisting of one or more plasma wave species (see, e.g., Miller & Ramaty 1987; Steinacker & Miller 1992; Hamilton & Petrosian 1992) is often suggested as the acceleration mechanism and has yielded relatively successful models. However, a common objection to previous work is that it has employed high-frequency waves such as whistlers, lower hybrid waves, or electron plasma waves. While these waves are quite efficient at accelerating electrons (Melrose 1980, chap. 8), their generation is problematic, since the typical way in which they are excited is through a resonant velocity-space instability that requires the preexistence of the same energetic electrons that one is trying to produce (see Gary 1993). Nonresonant instabilities may also generate the required waves, but they still require specific anisotropic particle distributions.

This "chicken-and-egg" problem can be avoided by beginning with a wave species that is generated independent of the energetic particles. Attractive candidates are the MHD modes. These waves can be produced by either large-scale restructuring of the magnetic field, which presumably occurs during the flare energy release phase, or by a shear in the plasma bulk velocity (Roberts et al. 1992), which would likely be found in regions of reconnection-driven plasma outflows (see, e.g., LaRosa & Moore 1993; Forbes 1996). The issue is now whether these waves can accelerate electrons from thermal energies.

Initial research into stochastic electron acceleration by MHD waves has yielded contradictory conclusions (e.g., contrast Eichler 1979, in the negative, to Achterberg 1979, 1981), but it has recently become evident through many additional studies that electron acceleration will indeed occur for both large-amplitude (Gisler & Lemons 1990; Gisler 1992; LaRosa, Moore, & Shore 1994; LaRosa et al. 1996) and small-amplitude (Miller, LaRosa, & Moore 1996; hereafter MLM) waves. The specific MHD mode that yields electron acceleration is the fast mode, propagating obliquely with respect to the ambient magnetic field, $\boldsymbol{B}_0$. Large-amplitude waves yield classic Fermi acceleration (Fermi 1949) and can (LaRosa et al. 1994, 1996) energize enough electrons above 20 keV to account for impulsive solar flare energy release fragments (ERFs) (Kiplinger et al. 1983; Machado et al. 1993).

Small-amplitude waves yield what is commonly called transit-time acceleration (Fisk 1976; Stix 1992), which is basically resonant Fermi acceleration (see § 2.1). Miller and coworkers (MLM) have shown with a self-consistent wave-particle treatment that low-amplitude, fast mode waves can rapidly accelerate electrons from the thermal distribution to MeV energies. With an injection of ≈ 10 ergs cm^{-3} ($\delta B/B_0 \sim 0.03$) of turbulence at any scale less than $\approx 10^8$ cm and over any time interval less than ≈ 1 s, the rate at which electrons are accelerated beyond 20 keV is consistent with that inferred for ERFs. Transit-time acceleration thus appears to be a very efficient and robust electron energization mechanism under flare conditions.

Miller and coworkers (MLM) used quasi-linear theory (QLT) to treat electron acceleration and assumed that the electron distribution remained isotropic in order to simplify the momentum diffusion equation. Unfortunately, isotropy also maximizes the transit-time acceleration rate. In the present paper we consider how transit-time acceleration fares under solar flare conditions without isotropizing scat-

tering and also examine the validity of QLT for this process with test-particle simulations. We give in § 2 a more detailed description of transit-time acceleration, a derivation of the orbit equations used in the simulations, and the quasi-linear theory for the process. In § 3 we present the results of the simulations and the quasi-linear analysis. A discussion of the results and a summary appear in §§ 4 and 5, respectively.

2. THEORY

In this section, we first present the basic physics of transit-time acceleration and point out the similarities and differences it has with Fermi acceleration. We next derive slow timescale equations of motion for an electron in the presence of a spectrum of fast mode waves; these orbit equations yield trajectories that are in excellent agreement with those determined by directly integrating the exact Lorentz force law, but they are integrated with orders of magnitude fewer computations. This section concludes with a discussion on the construction of discrete wave spectra and a derivation of the QLT diffusion coefficients.

2.1. *Basic Physical Mechanism*

The mechanism by which oblique fast mode waves accelerate particles is straightforward but subtle. One such wave has a parallel magnetic field component, which results in a series of compressive and rarefactive magnetic perturbations moving along $\boldsymbol{B}_0$ with the parallel wave speed $\omega/k_\parallel$, where ω is the wave frequency, and $k_\parallel$ is the component of the wavevector $\boldsymbol{k}$ along $\boldsymbol{B}_0$. In the frame travelling along $\boldsymbol{B}_0$ with speed $\omega/k_\parallel$ (wave frame), these perturbations are stationary, and the parallel particle velocity, $v'_\parallel$, will be affected by the usual mirror force, $-M\nabla_\parallel B$. Here, $M = mv_\perp^2/2B$ is the magnetic moment, m is the particle mass, $v_\perp$ is the particle velocity component normal to $\boldsymbol{B}_0$ (the same in both the wave and plasma frames), and B is the total (ambient plus wave-parallel) magnetic field.

For large-amplitude waves, essentially all electrons will be reflected by a compression in the wave frame. In the plasma frame, an electron then makes either a head-on or overtaking collision with a moving magnetic mirror, which leads to either a gain or loss of energy, respectively. Since the frequency of head-on collisions is greater than that for trailing collisions as a result of the larger relative velocity (see, e.g., Landau & Lifshitz 1962) between particle and wave, there will be a net gain of energy. This is just second-order Fermi acceleration (Fermi 1949). As a result of the large disparity between the mirror speed, $\omega/k_\parallel$, and the proton thermal speed for flare conditions, a negligible number of protons will be Fermi accelerated for realistic wave amplitudes (LaRosa et al. 1996). Hence, large-amplitude, fast mode waves will preferentially Fermi accelerate electrons.

As the wave amplitude decreases, a particle's pitch angle in the wave frame must approach 90° in order to ensure that reflection occurs before the particle has left the compression. Equivalently, $v'_\parallel$ must approach zero, which in the plasma frame implies that the parallel component of velocity, $v_\parallel$, is $\approx\omega/k_\parallel$. Thus, for small amplitude waves, an appreciable interaction between a wave and a particle arises only when the particle is moving at nearly the wave parallel phase speed. The interaction is now resonant, and $\omega - k_\parallel v_\parallel \approx 0$ is just the usual $\ell = 0$ (or Landau) resonance condition. However, given that resonance does occur, the subsequent physics is close to that of Fermi acceleration: particles with $v_\parallel$ slightly greater than $\omega/k_\parallel$ suffer a trailing collision with a wave compression and slow down; particles with $v_\parallel$ slightly less than $\omega/k_\parallel$ are struck by a compression and speed up.

However, there are two key differences between this resonant process and (nonresonant) Fermi acceleration. The first is that a spectrum of waves is now necessary for large energy gains. Using the fast mode wave dispersion relation, the resonance condition can be written as $v_\parallel = v_A/\eta$, where v_A is the Alfvén speed, and η is the cosine of the wave propagation angle. Resonance from Alfvénic to relativistic energies thus requires waves with propagation angles ranging from $\approx 0°$ to $\approx 90°$ for $v_\parallel > 0$ and from slightly more than 90° to $\approx 180°$ for $v_\parallel < 0$.

The second is the crucial role played by resonance overlap. Suppose there is a single (i.e., monochromatic) wave with a given parallel phase speed, $\omega/k_\parallel$, and a particle with $v_\parallel$ slightly greater than this. The particle will then suffer a trailing collision with some compression (call it No. 1) in the wave train and be slowed down. The compression one parallel wavelength behind No. 1 will then strike a slightly slower particle and speed it up. The particle will then suffer a trailing collision with No. 1 again and slow down. The process continues, with the particle oscillating in parallel speed about $\omega/k_\parallel$. Clearly, the same thing occurs if $v_\parallel$ is slightly less than $\omega/k_\parallel$ initially. Viewed in the wave frame, the particle bounces between two neighboring compressions about the minimum of a rarefaction. Since the mirror force drives this motion, oscillation will occur even if $v_\parallel$ is exactly $\omega/k_\parallel$, unless the particle is initially at the rarefaction minimum (where the mirror force is zero). The frequency of oscillation is referred to as the bounce frequency, ω_b (see, e.g., Karimabadi et al. 1990). Trapping or resonance will only occur if $v_\parallel$ is such that the frequency mismatch $|\omega - k_\parallel v_\parallel|$ is less than $2\omega_b$ (Karimabadi, Krauss-Varban, & Terasawa 1992).

As $v_\parallel$ deviates from $\omega/k_\parallel$, the particle will make further excursions from the rarefaction minimum and will eventually reach the compressive maximum. When this occurs, the particle will not be trapped in a single region and will instead travel along the entire wave train. Note that while $v'_\parallel$ (and thus $v_\parallel$) will be periodic as a result of (incomplete) adiabatic focusing and mirroring, it will not vary about a mean of $\approx\omega/k_\parallel$. The maximum difference between $v_\parallel$ and $\omega/k_\parallel$ (or between $v'_\parallel$ and zero) such that trapping or resonance can still occur is called the trapping width, $\Delta v_\parallel$. One would therefore expect that another condition for resonance is $|v_\parallel - (\omega/k_\parallel)| < \Delta v_\parallel$. In the Appendix, we derive nonrelativistic expressions for $\Delta v_\parallel$ and ω_b and show that this condition and the one on the frequency mismatch are identical.

A single wave will therefore yield only bounded periodic motion. The situation is quite different in a spectrum, however. If the periodic motion associated with one wave brings $v_\parallel$ of the particle to within a trapping width of a neighboring wave, the particle can resonate with that wave. This is referred to as resonance overlap. If the average $v_\parallel$ resulting from the second wave (equal to $\omega/k_\parallel$) is greater than that for the first, the particle will have a net gain of parallel energy. The process can continue with a third wave whose $\omega/k_\parallel$ is greater than that of the second. If there are many waves present, the particle can then "jump" from one resonance to the next and figuratively climb the parallel

energy ladder. It can also descend the ladder, but over time the particle will stochastically gain energy. In a continuous wave spectrum, resonance overlap automatically occurs; a discrete wave spectrum may or may not have overlap, depending on the frequency spacing of the waves and their amplitude.

This process could be called resonant Fermi acceleration, but the usual term for it is transit-time acceleration. The name arises because the resonance condition can be rewritten as $\lambda_\parallel/v_\parallel \approx T$, where T is the wave period, and $\lambda_\parallel = 2\pi/k\eta$ is the parallel wavelength. In other words, a wave and a particle will interact strongly when the particle transit time across the wave compression is approximately equal to the period.

Like Fermi acceleration, this resonant process preferentially accelerates electrons under flare conditions. The threshold speed for resonance is v_A, which is $\approx 0.04c$ for flares. A probable initial plasma temperature is 3×10^6 K (Reames, Meyer, & von Rosenvinge 1994), so that the electron and proton thermal speeds are $0.03c$ and $0.007c$, respectively. Since the threshold speed is ≈ 6 times the proton thermal speed, only a small number of protons can resonate with the waves. On the other hand, the threshold speed is comparable to the electron thermal speed, and so a large fraction of these particles will be energized. Also, while both processes increase only the parallel energy of the particle, the perpendicular energy plays a large role in this energization: from the mirror force and Newton's second law, $\dot{v}_\parallel$ is proportional to $v_\perp^2$, where the dot denotes differentiation with respect to time t (also see the Appendix). Hence, while not necessary for energization, any process (viz., pitch-angle scattering) that increases $v_\perp$ will clearly greatly increase the acceleration efficiency. We clarify here our meaning of pitch-angle scattering. In transit-time acceleration, $v_\parallel$ and hence the pitch angle will vary stochastically, but the pitch angle will likely decrease in a given time interval. By pitch-angle scattering, we refer to an ancillary process (such as Coulomb collisions or gyroresonant interactions) in which the pitch angle is more or less randomized between two limits (usually 0° and 180°) in a given time interval, with no strong systematic component.

If the distribution of parallel particle velocities always has a negative (positive) slope for $v_\parallel > 0$ ($v_\parallel < 0$), the number of particles slightly slower than $\omega/k_\parallel$ is greater than the number slightly faster than $\omega/k_\parallel$. More particles will gain energy than lose it, and the wave will be damped. Transit-time damping has been referred to as the magnetic analog of Landau damping (of a wave parallel electric field). While the two processes have obvious similarities, a significant difference is that the efficiency of the magnetic interaction can be increased by pitch-angle scattering. This affords transit-time damping the possibility of energizing particles far more rapidly than Landau damping and of leading to acceleration instead of heating.

2.2. *Slow Timescale Orbit Equations*

Consider an ionized hydrogen plasma permeated by a static magnetic field, $\boldsymbol{B}_0 = B_0\,\hat{\boldsymbol{z}}$, and containing a discrete spectrum of N monochromatic MHD fast mode waves. For simplicity, we assume that each wave is propagating in the x-z plane. The wave electric field is linearly polarized and lies along the y-axis, while the magnetic field has both a z (parallel or compressive) and an x component. In a gauge where the scalar potential is zero, the vector potential of wave i is given by

$$\boldsymbol{A}_i = \frac{cE_i}{\omega_i}\,\hat{\boldsymbol{y}}\,\cos\,\varphi_i\,, \tag{2.1}$$

where the phase, φ_i, equals $k_{\perp i}x + k_{\parallel i}z - \omega_i t + \varphi_{0i}$. The quantities $\boldsymbol{k}_i = k_{\perp i}\hat{\boldsymbol{x}} + k_{\parallel i}\hat{\boldsymbol{z}}$, E_i, ω_i, and φ_{0i} are the wavevector, electric field magnitude, frequency, and constant phase offset, respectively.

Substituting the total vector potential, $-yB_0\,\hat{\boldsymbol{x}} + \sum_{i=1}^{N}\boldsymbol{A}_i$, into the relativistically correct Hamiltonian, H, for an electron of charge $-e$, mass m, and cyclotron frequency $\Omega = eB_0/mc$, transforming to guiding-center action-angle variables (Ginet & Heinemann 1990), expanding H to first order in E_i, and then expanding terms like $\cos(a + b\sin\theta)$ in terms of Bessel functions, we eventually find that

$$H = \gamma mc^2 + \frac{mc^2}{\gamma}\left(\frac{P_\perp}{mc}\right) \times \sum_{i=1}^{N}\epsilon_i \sum_{\ell=-\infty}^{+\infty} J'_\ell(k_{\perp i}\rho)\,\sin\,(k_{\parallel i}z - \omega_i t + \ell\theta + \delta_i)\,, \tag{2.2}$$

where the dimensionless electric field, ϵ_i, is equal to $eE_i/mc\omega_i$, J'_ℓ is the Bessel function derivative, and δ_i is a constant (containing φ_{0i}). The action-angle pair is (J, θ) with $P_\perp = (2Jm\Omega)^{1/2}$ and $\rho = P_\perp/m\Omega$. In the limit of vanishingly small E_i, $P_\perp$ and ρ become the perpendicular mechanical momentum, $p_\perp$, and gyroradius in the guiding center frame, respectively. The other canonical pair is $(p_\parallel, z)$, where $p_\parallel$ is both the canonical and mechanical momentum. The quantity $\gamma = [(p_\parallel/mc)^2 + (P_\perp/mc)^2 + 1]^{1/2}$ and becomes the usual Lorentz factor when $E_i \to 0$. With another canonical transformation to eliminate time, the Hamiltonian has the same form as that for a simple harmonic oscillator (see also Lichtenberg & Lieberman 1983), as expected from the above discussion.

We have basically decomposed the Hamiltonian into resonant contributions. The harmonic number of interest for transit-time acceleration is $\ell = 0$, in which case θ is cyclic, $\dot{J} = 0$, and the canonical variable, $P_\perp$, is constant. Also, since the fast angle, θ, describes gyromotion, the Hamiltonian for $\ell = 0$ is also on an intrinsically slow timescale. (For other harmonic numbers, the Hamiltonian would need another canonical transformation to a rotating coordinate system along with an averaging over θ in order to become a slow timescale Hamiltonian.) Using the Hamilton equations for $(p_\parallel, z)$, and approximating $P_\perp$ by $p_\perp$, we then have that

$$\dot{p}_\perp = 0\,, \tag{2.3a}$$

$$\dot{p}_\parallel = -\frac{mc^2}{\gamma}\left(\frac{p_\perp}{mc}\right)\sum_{i=1}^{N}\epsilon_i k_{\parallel i} J'_0(k_{\perp i}\rho)\,\cos\,(k_{\parallel i}z - \omega_i t + \delta_i)\,, \tag{2.3b}$$

and

$$\dot{z} = \frac{p_\parallel}{m\gamma} - \frac{p_\parallel}{m\gamma^3}\left(\frac{p_\perp}{mc}\right)\sum_{i=1}^{N}\epsilon_i J'_0(k_{\perp i}\rho)\,\sin\,(k_{\parallel i}z - \omega_i t + \delta_i)\,. \tag{2.3c}$$

It is consistent with $P_\perp \to p_\perp$ to take $p_\perp$ to be the perpendicular momentum in the plasma frame. These equations

are not appropriate for Fermi acceleration, where the large-amplitude waves are not consistent with the above expansion of H to first order in E_i.

The quantity $k_{\perp i}\rho$ is $\ll 1$ for the waves and electrons under consideration, and so the Bessel function derivative can be accurately approximated by $k_{\perp i}\rho/2$. Since the wave magnetic field amplitude, B_i, is larger than E_i by a factor $c/v_A \gg 1$, the bulk of the wave field energy is in the magnetic field, and it is more convenient to specify B_i. Rewriting equations (2.3a)–(2.3c) in terms of B_i, employing the fast mode wave dispersion relation, and transforming to dimensionless variables, we then obtain

$$\frac{d\tilde{p}_\parallel}{d\tilde{t}} = -\frac{\tilde{p}_\perp^2}{2\gamma}\sum_{i=1}^{N}\tilde{B}_i\tilde{k}_i\eta_i(1-\eta_i^2)^{1/2}\cos\left(\tilde{k}_{\parallel i}\tilde{z}-\tilde{\omega}_i\tilde{t}+\delta_i\right), \tag{2.4a}$$

$$\frac{d\tilde{z}}{d\tilde{t}} = \frac{\tilde{p}_\parallel}{\gamma} - \frac{\tilde{p}_\parallel}{\gamma^3}\left(\frac{\tilde{p}_\perp^2}{2}\right)\sum_{i=1}^{N}\tilde{B}_i(1-\eta_i^2)^{1/2}\sin\left(\tilde{k}_{\parallel i}\tilde{z}-\tilde{\omega}_i\tilde{t}+\delta_i\right). \tag{2.4b}$$

The dimensionless or normalized variables (denoted by a tilde) are as follows: $\tilde{B}_i = B_i/B_0$, $\tilde{p} = p/mc$, $\tilde{v} = v/c$, $\tilde{t} = t/T_H$, $\tilde{z} = \Omega_H z/c$, $\tilde{k} = ck/\Omega_H$, and $\tilde{\omega} = \omega/\Omega_H$, where Ω_H is the hydrogen cyclotron frequency. We normalize time with respect to the hydrogen cyclotron period, $T_H = \Omega_H^{-1}$, since this is much closer to the acceleration timescale than the electron cyclotron period and also yields normalized wave frequencies and wavenumbers close to unity.

We have numerically integrated equations (2.4a) and (2.4b) and compared the results to those obtained by integrating the exact Lorentz equations of motion. We find that equations (2.4a) and (2.4b) yield accurate orbits when the time step is smaller than about 0.01 times the bounce period of the particle. In other words, the time step needs to be small enough to resolve the slow timescale motion of the particle, which in this case is the periodic motion between two compressions. For the cases considered in the next section, the time step is typically about equal to T_H. The Lorentz equations, on the other hand, which resolve the gyromotion, require time steps of at least 0.1 times the electron cyclotron period, Ω^{-1}. Hence, for a given final time, the Lorentz equations require about 18,000 times more time steps than the slow timescale equations. Furthermore, in the Lorentz case, there are six coupled equations (three for the momentum components and three for the position components), as opposed to only two for the slow timescale case, so that each time step requires much more computation as well. We have explored various numerical integration techniques for equations (2.4a) and (2.4b) and have found that second-order Runge-Kutta is best. For instance, both second- and fourth-order R-K yield correct results for time steps $\lesssim T_H$, and inaccuracies occur in both cases for about the same, larger time step. However, second-order R-K involves fewer computations and is faster. First-order R-K is generally a disaster.

2.3. *Wave Spectrum and Diffusion Coefficients*

In many physical situations, like flares, the details of the wave spectrum are not known. De La Beaujardière & Zweibel (1989) and Zweibel & de La Beaujardière (1990) consider discrete spectra composed of waves that are normal modes of a cylindrical flare flux tube. Since test-particle simulations involve the solution of orbit equations (Lorentz or slow timescale) for a discrete spectrum of waves, such spectra can be used directly. We assume a more generic geometry and consider wave spectra that are continuous (but possibly bounded) in both wavenumber and propagation angle. Our first issue in doing a test-particle simulation then becomes constructing a discrete spectral density that mimics the continuous one, at least as far as particle motion is concerned. In light of the discussion in § 2.1, a fundamental requirement of such a discrete spectral density is that resonance overlap occurs between neighboring waves. If this condition is not satisfied for two neighboring waves, a particle will be unable to jump between them and unable to resonate at any higher energy. In the extreme case in which overlap does not occur between waves that are resonant with low-energy particles, there will be essentially no acceleration at all. A discrete spectrum with a resonance "gap" will not mimic any continuous spectrum, where resonance overlap automatically occurs. Hence, if a spectrum is to be constructed in a certain k and η range, a given wave must have resonance overlap with the waves nearest to it in k and η. This is true for any resonance and not just $\ell = 0$. Of course, if the physical wave spectrum is discrete to begin with, then gaps may occur, and acceleration in that case is fundamentally limited.

Evaluation of the overlap criterion requires the trapping width for a particle and wave. Using Karimabadi & Menyuk (1991), we find that the momentum trapping half-width, $\Delta p_{\parallel i}/2$, for a particle and monochromatic fast mode wave, i, is given by

$$\left(\frac{\Delta\tilde{p}_{\parallel i}}{2}\right)^2 = \frac{\tilde{p}_\perp^2}{2}\frac{\eta_i^2(1-\eta_i^2)^{1/2}}{\eta_i^2-\tilde{v}_A^2}\tilde{B}_i, \tag{2.5}$$

where the cosine of wave i propagation angle, η_i, is $v_A/v_\parallel$. Note that for a fixed B_i, the trapping width increases with increasing wave propagation angle (and thus $v_\parallel$). The bounce frequency for wave i is given by

$$\left(\frac{\tilde{\omega}_{bi}}{\tilde{k}_{\parallel i}}\right)^2 = \frac{1}{2}\left(\frac{\tilde{p}_\perp}{\gamma}\right)^2\frac{\eta_i^2-\tilde{v}_A^2}{\eta_i^2}(1-\eta_i^2)^{1/2}\tilde{B}_i. \tag{2.6}$$

For $\omega/k_\parallel \ll c$ and $p \ll mc$, these expressions reduce to those found in the Appendix. They also agree well with those obtained from a numerical solution of the orbit equations (eqs. [2.4a]–[2.4b]). De La Beaujardière & Zweibel (1989) derived the bounce frequency and trapping half-width when the waves are normal modes of a cylindrical tube of plasma.

The momentum diffusion coefficient in the parallel direction, $D_{\parallel\parallel}$, can be obtained from equation (2.4a) by first calculating the correlation function and then performing a time integration, and it is given by equation (A8) in MLM (approximating the J_0' as above). This expression for the diffusion coefficient contains the delta function, $\delta(\omega_i - k_{\parallel i}v_\parallel)$, and is not appropriate for a discrete wave spectrum. In this case, the resonance must be broadened, which amounts to saying that the frequency mismatch need not be exactly zero in order for an interaction to occur. In light of the above discussion on trapping widths, this is to be expected. According to the Karimabadi & Menyuk (1991) resonance-broadening theory, $D_{\parallel\parallel}$ for a discrete wave spectrum is given by replacing the delta function with a broadening function, so that

$$\tilde{D}_{\parallel\parallel} = \frac{\pi}{8}\frac{\tilde{p}_\perp^4}{\gamma^2}\sum_{i=1}^{N}\eta_i^2\tilde{B}_i^2\tilde{k}_{\perp i}^2 f_i, \tag{2.7}$$

where $\tilde{D}_{\parallel\parallel} = D_{\parallel\parallel}/(mc)^2\Omega_H$, and the broadening function, f_i, is equal to $1/4\tilde{\omega}_{bi}$ if $|\tilde{\omega}_i - \tilde{k}_{\parallel i}\tilde{v}_\parallel| \le 2\tilde{\omega}_{bi}$ and equal to 0 otherwise. Depending on the spacing of the waves, more than one wave can contribute to the sum for a given $v_\parallel$.

If the wave spectrum is continuous, the spectrum can be described by a spectral density, $\tilde{W}_B(\tilde{k}, \eta)$, such that $(B_0^2/8\pi)\int_0^\infty d\tilde{k}\int_{-1}^{+1} d\eta \tilde{W}_B(\tilde{k}, \eta)$ is the total magnetic energy density, U_B, of the waves. The diffusion coefficient in this case can be found from that for a discrete spectrum without resonance broadening (eq. [A8] of MLM) by replacing the summation over the number of waves with an integration over k and η and then evaluating the integral over η using the delta function. The spectral density in flares in unknown, and we assume it to be a separable function for simplicity. In this case,

$$\tilde{D}_{\parallel\parallel} = \frac{\pi}{4}\frac{\tilde{p}_\perp^4}{\gamma^2|\tilde{v}_\parallel|^3}\left(1 - \frac{v_A^2}{v_\parallel^2}\right)\tilde{v}_A^2\langle\tilde{k}\rangle\tilde{W}_B(\eta_r)\,, \qquad (2.8)$$

where $\langle\tilde{k}\rangle$ is the mean wavenumber of the waves, and $\eta_r = v_A/v_\parallel$ is the propagation angle cosine of the wave resonant with an electron of parallel speed, $v_\parallel$. The $\int_{-1}^{+1} d\eta \tilde{W}_B(\eta)$ is the normalized total magnetic energy density of the waves, $\tilde{U}_B = U_B/U_0$, where $U_0 = B_0^2/8\pi$. In equation (2.8), $v_\parallel$ must be greater than v_A; otherwise, the diffusion coefficient is zero. In equation (2.7), $v_\parallel$ can be less than v_A and still produce a nonzero $D_{\parallel\parallel}$, as long as the particle is within a trapping width of a wave.

3. RESULTS

In this section we compare test-particle simulations with quasi-linear predictions. Since the diffusion coefficient and hence the acceleration rate depend only on $\langle k\rangle$ and not the detailed spectral energy distribution in k-space, we place all the waves at the same wavenumber, k_0. This also simplifies the evaluation of the resonance overlap condition, since now only η of the waves will change. We take the Alfvén speed to be $0.036c$, and $B_0 = 500$ G (which implies a density of 10^{10} cm^{-3}). The Alfvén speed is the threshold speed for transit-time acceleration.

We constructed a test-particle code in which the orbits of an arbitrary number of electrons could be determined using equations (2.4a) and (2.4b), given the properties of the N fast mode waves. The code is parallelized, supplies much diagnostic data at user-specified intervals, and was run here on a dedicated Sun SPARC20MP 2-processor workstation. Even so, the simulations can easily be quite long. In the interest of confining them to reasonable periods of time, we were forced to treat only a relatively small number of particles. (For example, following 100 particles out to 0.1 s with 500 waves requires a week of CPU time on the above machine.) We thus cannot directly compare particle distributions and instead compare moments (Karimabadi & Menyuk 1991). We use specifically the first- and second-order central moments, or the mean and standard deviation, respectively.

Cases 1–3 deal with transit-time acceleration without pitch-angle scattering, while case 4 illustrates its effect on the acceleration rate. In all cases the waves are confined to positive η. As discussed in de La Beaujardière & Zweibel (1989), particle trajectories are stochastic when resonances overlap, and in general the equations of motion yield different results for different integration time steps. We use a time step small enough so that a smaller time step yields the same results out to the maximum time of the simulation.

3.1. *Case 1*

In this case, we take $\tilde{k}_0 = 10$, each electron to have $\tilde{p}_\perp = 0.032$, and each wave to have the same small amplitude, $\tilde{B}_i = 0.05$. This value of $p_\perp$ is the thermal momentum at 3×10^6 K. With the above value of v_A, the frequency of each wave, $\tilde{\omega}_i$, is then 0.36, which is about the maximum frequency fast mode waves can have and still possess the simple, low-frequency MHD properties previously discussed and upon which our results in §§ 2.2 and 2.3 are predicated. Each wave is assigned a constant δ_i chosen randomly from 0 to 2π. The only thing left to specify for the discrete wave spectrum is η_i for each wave, which we do as follows: we first calculate $\eta_r = v_A/v_\parallel$ for $v_\parallel = v_1 = 0.037c$ (just above the threshold speed). This is η_1. We then find the trapping width, $\Delta v_{\parallel 1}$, for this wave from equation (2.5). The resonant parallel velocity for the second wave must be in this trapping width. We next determine $v_2 = v_1 + \xi\Delta v_{\parallel 1}$, where ξ is some parameter less than unity, which we take equal to 0.15 to be on the safe side. Then, $\eta_2 = v_A/v_2$. We then find the trapping width for this wave, find v_3 by increasing v_2 by $\xi\Delta v_{\parallel 2}$, and then take $\eta_3 = v_A/v_3$. The process continues until a velocity of about c is reached.

The result of this procedure is a discrete spectrum in which resonance overlap is not only guaranteed but in which an electron will typically resonate with several waves at once. Here, the spectrum consists of 502 waves with η ranging from ≈ 0 to ≈ 1 and with a total magnetic energy density of $\tilde{U}_B = 0.63$.

Figure 1 gives the details of the spectrum. We bin the waves in η and present in Figure 1*a* the resulting spectral density, $W_B(\eta)$. The spectral density is not uniform: there is a concentration of wave energy and thus waves at large propagation angles. Figure 1*b* shows the number of waves that are resonant with an electron of parallel momentum, $p_\parallel$. As a result of the wave-selection process, this number is about constant over an order of magnitude but does fall off at higher $p_\parallel$ as a result of a decreasing bounce frequency. The diffusion coefficient for this discrete spectrum is found from equation (2.7) and is given in Figure 1*c*. Note that $D_{\parallel\parallel}$ decreases with increasing $p_\parallel$ over most of the range. As $p_\parallel$ increases, so does the parallel wavelength, $\lambda_\parallel$, of the resonant waves. Since the scale of the magnetic compression increases, so does the mirroring time, so that the electron can make fewer collisions in a given interval of time. This results in a decrease of the rate of change of $p_\parallel$ and thus $D_{\parallel\parallel}$. The larger amount of wave energy that is available to large-$p_\parallel$ electrons is not sufficient to offset this effect.

We inject 100 electrons into this discrete wave spectrum, with random initial parallel momenta, $\tilde{p}_\parallel$, in the interval 0.037–0.047. Equations (2.4a) and (2.4b) are then solved for each electron, using a time step of $1T_H$. The mean, $\langle p_\parallel\rangle$, and standard deviation, σ, of the resulting distribution of parallel momenta are shown as a function of time, t, in Figure 2 (*solid lines*). Acceleration is rapid, with the average parallel energy reaching ≈ 140 keV in ≈ 0.4 s.

The continuous wave spectrum modeled by this discrete one is given by the spectral density in Figure 1*a*. The corresponding diffusion coefficient is found from equation (2.8) (where we have fit $W_B[\eta]$ in order to prevent jumps in the value) and is shown in Figure 1*c*. The close agreement between the two coefficients for most $p_\parallel$ is the best proof of the equivalency of the discrete and continuous wave

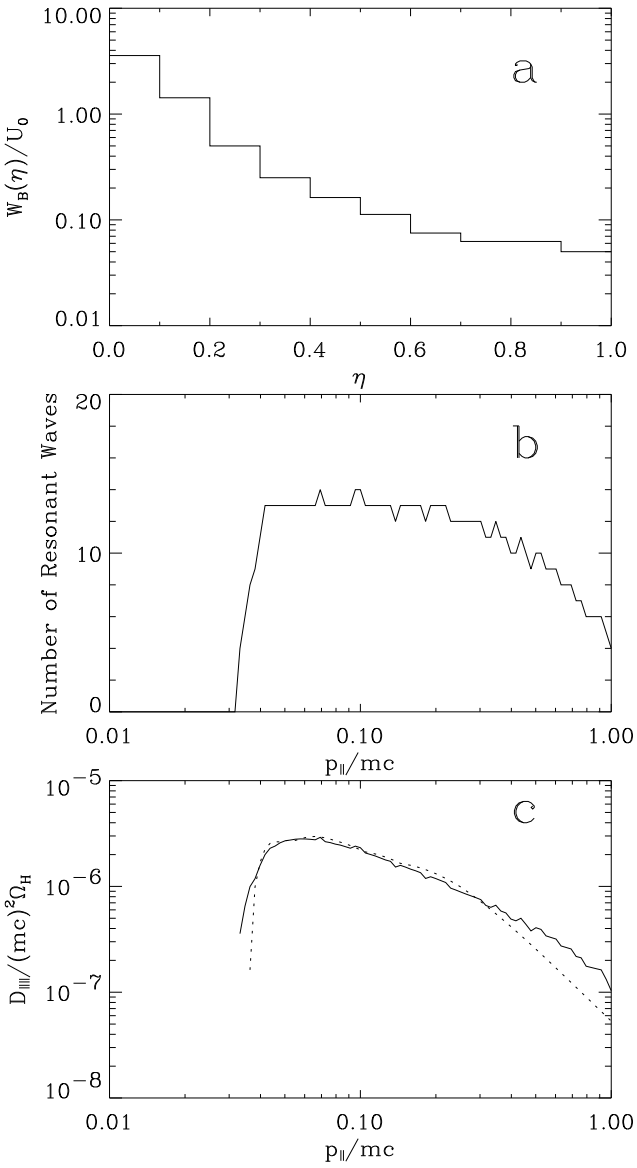

FIG. 1.—Spectral density, number of resonant waves, and diffusion coefficient for case 1. (*a*) The η-dependent spectral density, normalized to the ambient magnetic field energy density, U_0. (*b*) Number of waves that are resonant with an electron of parallel momentum, $p_\parallel$. (*c*) The diffusion coefficients for the discrete wave spectrum (*solid line*) and for a continuous wave spectrum having the spectral density in (*a*) (*dotted line*).

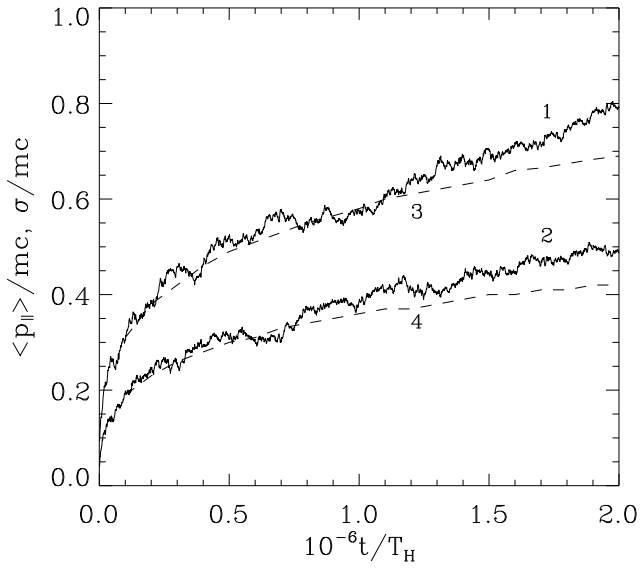

FIG. 2.—Time-dependent mean, $\langle p_\parallel \rangle$, and standard deviation, σ, of the electron distribution for case 1. Lines 1 and 2: $\langle p_\parallel \rangle$ and σ, respectively, from the test-particle simulation. Lines 3 and 4: $\langle p_\parallel \rangle$ and σ, respectively, from QLT. The H cyclotron period, T_H, equals 2.1×10^{-7} s.

spectra, at least as far as their effect on particles is concerned. The electron distribution function, $f(p_\parallel)$, in QLT evolves according to the diffusion equation

$$\frac{\partial f}{\partial t} = \frac{\partial}{\partial p_\parallel} D_{\parallel\parallel} \frac{\partial f}{\partial p_\parallel} . \tag{3.1}$$

With the continuous-spectrum $D_{\parallel\parallel}$, we transform to dimensionless variables and numerically solve this equation with fully implicit finite differencing. The initial distribution is uniform between $\tilde{p}_\parallel = 0.037$ and 0.047 and normalized to unity. We then determine $\langle p_\parallel \rangle = \int_0^\infty dp_\parallel\, p_\parallel f$ and $\sigma^2 = \int_0^\infty dp_\parallel (p_\parallel - \langle p_\parallel \rangle)^2 f$ as a function of time. The results are shown in Figure 2 (*dashed lines*). We obtain the same results if the discrete spectrum $D_{\parallel\parallel}$ is used instead of the continuous spectrum $D_{\parallel\parallel}$, as expected on the basis of their approximate equality. There is close agreement between the test-particle simulations and the predictions of QLT, with $\langle p_\parallel \rangle$ differing by no more than 13%.

The question at this point might now be, Is there any other discrete spectrum that can mimic the continuous spectrum given in Figure 1*a*? The answer is yes, and there is theoretically an infinite number of them. They can be obtained by simultaneously varying ξ and $\tilde{B}_i$ (with the other parameters held constant), such that the total wave energy density, U_B, remains the same. While this is a matter of trial and error, we can typically find a different discrete wave spectrum in only two or three tries. For example, with $\tilde{B}_i = 0.038$ and $\xi = 0.10$, we obtain a discrete spectrum of 863 waves. The spectral density, number of resonant waves, and diffusion coefficient for this discrete spectrum are shown in Figure 3. Figures 1*a* and 3*a* are almost identical, as are the discrete-spectrum diffusion coefficients in Figures 1*c* and 3*c*. Hence, both discrete spectra yield the same spectral density and the same diffusion coefficient, while differing substantially in the number of waves that are resonant with a given electron.

Since the $D_{\parallel\parallel}$ are the same, both discrete spectra will yield the same test-particle results, and in practice one would ideally chose the case that yielded the smaller simulation time. For example, the later case has more waves (which increases this time), but each has a smaller amplitude and a larger bounce period (so that greater time steps could be used). However, as a result of the bounce period being proportional to $B_i^{1/2}$, the number of waves increases by 73% while the time step (number of time steps) could only be increased (decreased) by about 14%. The first case is thus more desirable than the second. The factors that prevent decreasing the number of waves to very small values are $D_{\parallel\parallel}$, which becomes more irregular and jagged (see Figs. 1*c* and 3*c*), and the number of resonant waves, which must be at least a few to ensure a good resonance overlap. As long as these conditions are satisfied, no one discrete spectrum is more "correct" than another.

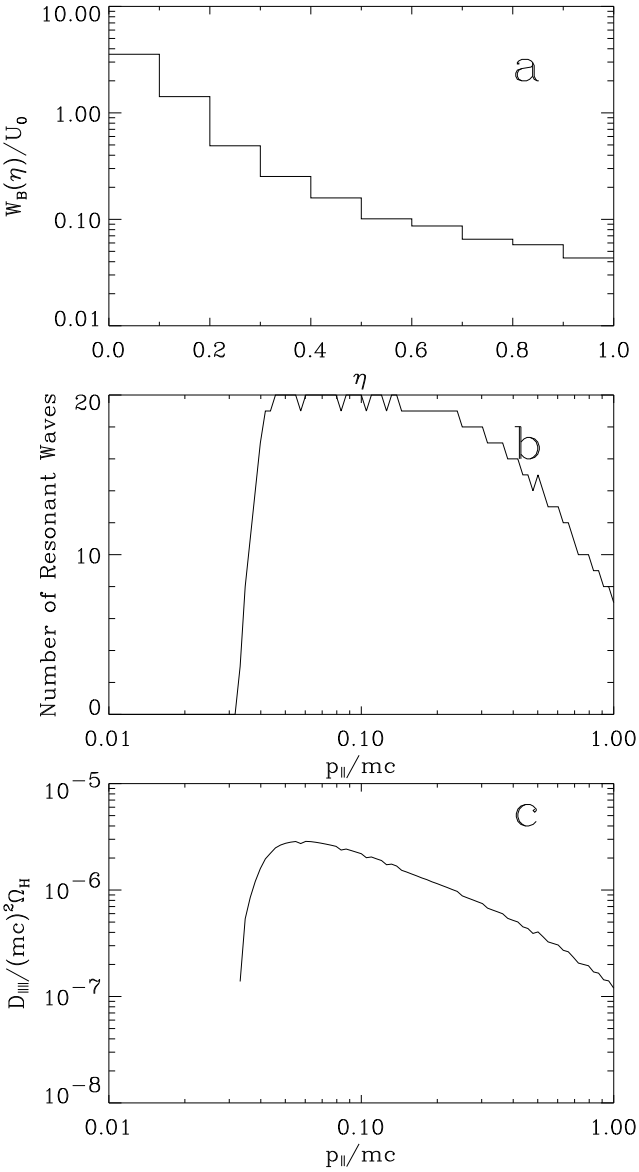

FIG. 3.—Spectral density, number of resonant waves, and diffusion coefficient for case 1 parameters, except that $\xi = 0.10$ and $\tilde{B}_i = 0.038$. The diffusion coefficient resulting from the continuous spectrum in (*a*) is not shown in (*c*), as it is the same as that in Fig. 1*c*.

3.2. *Case 2*

Here, the parameters have the same values as in case 1, except that $\tilde{k}_0 = 5$, and so $\tilde{\omega}_i = 0.18$. Each wave is assigned a constant δ_i chosen randomly from 0 to 2π and an η_i according to the procedure above. The resulting spectral density and number of resonant waves are identical to those in Figures 1*a* and 1*b*, respectively. The diffusion coefficients have the same form as those in Figure 1*c* but are a factor of 1/2 lower (e.g., from eqs. [2.7] and [2.6], $D_{\parallel\parallel}$ is proportional to $\tilde{k}_0$). We injected 100 electrons as above and calculated the mean and standard deviation of their $p_\parallel$, which we show in Figure 4. Energization is rapid in this case as well, with the particles reaching a mean parallel energy of ≈ 85 keV in about 0.4 s. We also show the same quantities as determined from a numerical solution of equation (3.1), using the diffusion coefficient for the discrete wave spectrum. The agreement between the test-particle and QLT results is excellent.

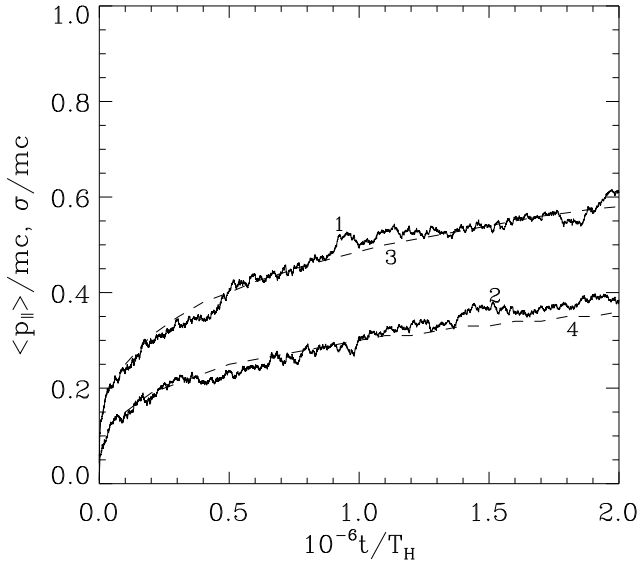

FIG. 4.—Same as Fig. 2, but for case 2

3.3. *Case 3*

The two previous cases had an anisotropic spectral density. To produce an isotropic one, the η_i are chosen so as to be uniformly spaced (for a constant B_i). Since the bounce frequency is relatively large for waves at high η, low-$p_\parallel$ electrons will be able to resonate with many waves at once. However, since the bounce frequency decreases for decreasing η, high-$p_\parallel$ electrons will experience a sharp decline in the number of resonant waves. For sufficiently high $p_\parallel$, this number will become zero (mostly as a result of the γ^{-1} dependence in the bounce frequency). This tendency was offset somewhat in the previous two cases by choosing waves according to the trapping width. It can be slightly offset in an isotropic case by choosing more waves. However, unless the number of waves is in the tens of thousands (a prohibitively large value), the value of $p_\parallel$ at which resonance overlap ceases will not extend much beyond mc (for small $p_\perp$). Moreover, the number of resonant waves will now be so large at low $p_\parallel$ (see below) that time steps $\ll T_H$ will need to be used for accuracy. Both issues place a serious practical limit on the maximum energies that can be obtained in a simulation.

In this case, we construct a spectrum consisting of 502 waves uniformly spaced in η from $\tilde{v}_A/0.99$ to $\tilde{v}_A/0.037$. The denominators are the maximum and minimum parallel velocities an electron can achieve, respectively. The amplitude is $\tilde{B}_i = 0.05$, and $\tilde{k}_0 = 5$. To aid in resonance overlap at high $p_\parallel$, we took $\tilde{p}_\perp = 0.05$. The spectral density, number of resonant waves, and diffusion coefficient are shown in Figure 5. The number of resonant waves at $\tilde{p}_\parallel \approx 0.05$ reaches almost 300, but it declines rapidly as $\tilde{p}_\parallel$ increases and eventually reaches zero at ≈ 0.7. This will be the upper limit on $\tilde{p}_\parallel$ for any simulation that employs this discrete spectrum. (Increasing the number of waves by a factor of 3, while lowering $\tilde{B}_i$, increases the upper limit on $\tilde{p}_\parallel$ to about 1; any limit higher than 1 requires at least an order of magnitude more waves.) In Figure 5*c*, the agreement between the $D_{\parallel\parallel}$ for the discrete spectrum and that for a continuous spectrum having the spectral density in Figure 5*a* is excellent all the way up to the maximum value of $p_\parallel$.

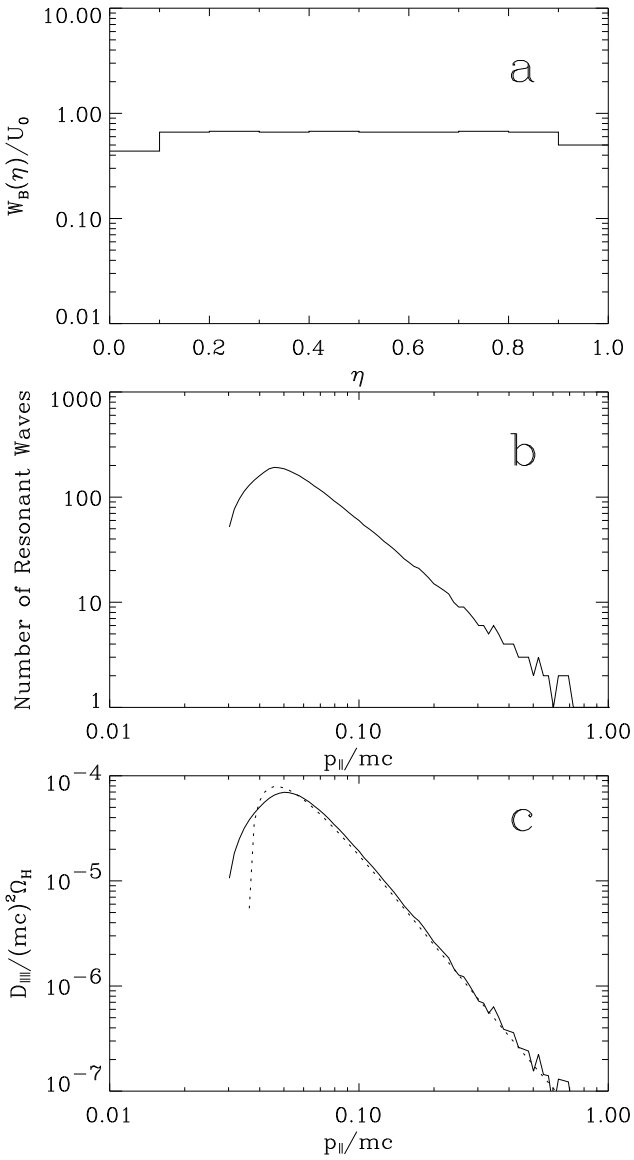

FIG. 5.—Same as Fig. 1, but for case 3

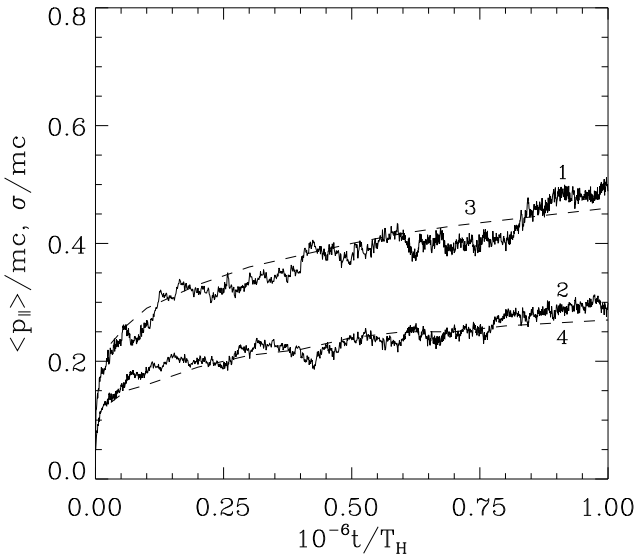

FIG. 6.—Same as Fig. 2, but for case 3

As before, we injected 100 electrons with initial $\tilde{p}_\parallel$ between 0.037 and 0.047 and followed their evolution. We needed to take time steps of $0.5T_H$ because of the large number of resonant waves at low $p_\parallel$, and so we evolved the particles only to $10^6 T_H$ in order to maintain the length of a simulation. These results are shown in Figure 6, along with those obtained by solving the diffusion equation with the discrete-spectrum diffusion coefficient in Figure 5*c*. The agreement between the orbit calculations and QLT is excellent, and the electrons achieve an average energy of ≈ 60 keV in ≈ 0.2 s.

3.4. *Case 4*

The strength of the interaction between a particle and resonant wave is proportional to the particle magnetic moment, M (eq. [2.4a]). Consequently, pitch-angle scattering, by transferring energy from the parallel to perpendicular direction, can dramatically increase the efficiency of transit-time acceleration (but note that energy gain is still only in the parallel direction). To illustrate, we performed a test-particle simulation using the discrete wave spectrum of case 2 and included isotropizing pitch-angle scattering.

We show in Figures 7*a* and 7*b* the parallel diffusion coefficient for this discrete wave spectrum for four different values of $p_\perp$. The $D_{\parallel\parallel}$ for $\tilde{p}_\perp = 0.032$ is one-half that shown in Figure 1*c*, as expected on the basis of the constant k_0 being one-half as large in this case. Aside from the diffusion coefficient increasing rapidly with increasing $p_\perp$, it also becomes nonzero for $v_\parallel < v_A$. In fact, except for $\tilde{p}_\perp = 0.032$, $D_{\parallel\parallel}$ is nonzero for some negative parallel velocities as well; hence, even though $k_\parallel > 0$, electrons can diffuse both parallel and antiparallel to $\boldsymbol{B}_0$. This is a consequence of the proportionality between the trapping width (or bounce frequency) and $p_\perp$, which allows large-$p_\perp$ electrons with $v_\parallel < v_A$ to still resonate with some of the waves in the spectrum. The large bounce frequencies at higher $p_\perp$ also lead to large numbers of resonant waves for $v_\parallel > 0$. For example, when $\tilde{p}_\perp = 10$ (curve 4), electrons with $0.01 \leq \tilde{p}_\parallel \leq 10$ typically resonate with ≈ 200–300 waves simultaneously, which is a substantial fraction of the total of 502.

The diffusion coefficients obtained from equation (2.8) using the continuous $W_B(\eta)$ (which is the same as that in Fig. 1*a*) are shown in Figure 7*c* for the same four values of $p_\perp$. As expected, there is excellent agreement between the discrete and continuous spectrum diffusion coefficients for $\tilde{p}_\perp = 0.032$, since this is the value used to construct the discrete spectrum in the first place. However, serious discrepancies arise at higher $p_\perp$. For the continuous spectrum, $D_{\parallel\parallel}$ is always confined to positive $p_\parallel$, and the threshold parallel momentum for resonance increases with increasing $p_\perp$. The first of these is due to the absence of trapping widths in the calculation of the diffusion coefficient, while the second results from $\tilde{p}_\parallel = \gamma\tilde{v}_\parallel$, which implies that the threshold, $\tilde{p}_\parallel$, is $\approx (1 + \tilde{p}_\perp^2)^{1/2}\tilde{v}_A$. Clearly, at these higher values of $\tilde{p}_\perp$, the discrete spectrum does not model the continuous spectrum in Figure 1*a*.

We thus conclude that the discrete wave spectrum used to model a given continuous one depends on the value of $p_\perp$. In retrospect, this is not surprising, since $p_\perp$ is an inte-

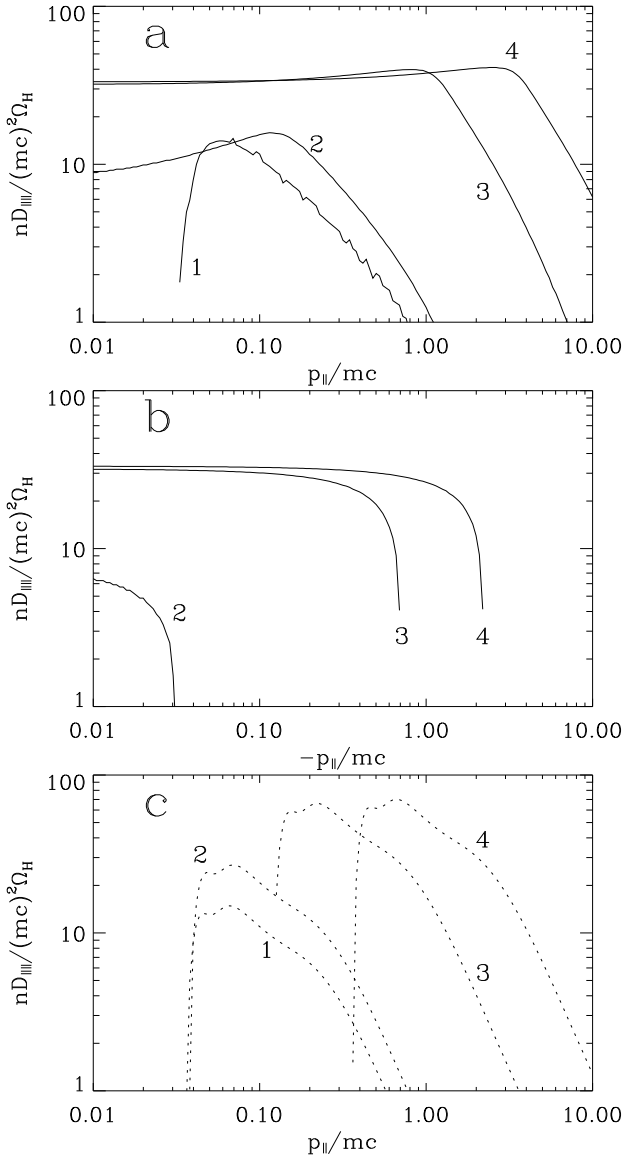

FIG. 7.—Parallel diffusion coefficients for the case 2 wave spectrum. (*a*) $D_{\parallel\parallel}$ from the discrete wave spectrum for four different values of $p_\perp$. Curve 1: $\tilde{p}_\perp = 0.032$, $n = 10^7$. Curve 2: $\tilde{p}_\perp = 0.32$, $n = 2000$. Curve 3: $\tilde{p}_\perp = 3.2$, $n = 10$. Curve 4: $\tilde{p}_\perp = 10$, $n = 1$. (*b*) Same as (*a*), except for negative $p_\parallel$. (*c*) $D_{\parallel\parallel}$ obtained from the continuous wave spectrum $W_B(\eta)$. Curves are as in (*a*) and (*b*), except $n = 5$ in curve 3, and $n = 0.5$ in curve 4.

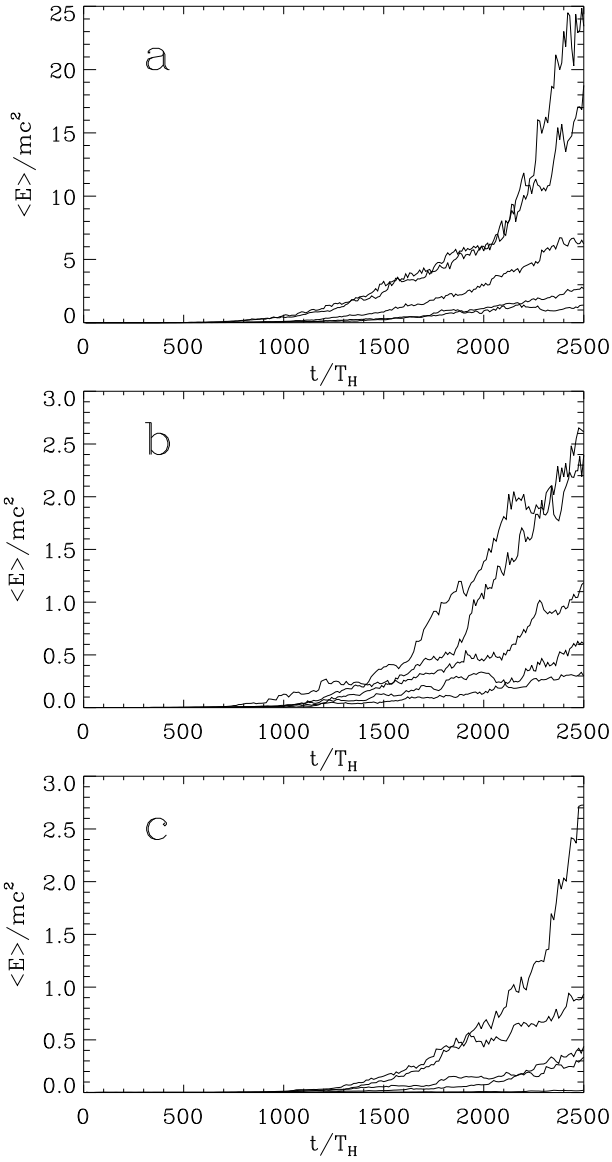

FIG. 8.—The average kinetic energy of 100 electrons as a function of time when pitch-angle scattering is included. (*a*) For the discrete wave spectrum used in case 2, where $\tilde{U}_B = 0.63$. Curves, from top to bottom, at $\tilde{t} = 2500$: $\tilde{\tau} = 12.5$, 25, 50, 100, and 6.25. (*b*) For a similar discrete wave spectrum but with $\tilde{U}_B = 0.306$. Curves, from top to bottom, at $\tilde{t} = 2500$ are $\tilde{\tau} = 12.5$, 25, 50, 100, and 6.25. (*c*) For a similar discrete wave spectrum but with $\tilde{k}_0 = 2.5$. Curves, from top to bottom, at $\tilde{t} = 2500$: $\tilde{\tau} = 25$, 50, 100, 12.5, and 6.25. The $\tilde{\tau} = 6.25$ curve is barely visible above the t-axis, and $\langle\tilde{E}\rangle = 0.022$ at $\tilde{t} = 2500$.

gral part of the construction of the discrete spectrum. Here, the continuous spectrum in Figure 1*a* is modeled by the case 2 discrete wave spectrum only for $\tilde{p}_\perp = 0.032$. At other values of $p_\perp$, a different discrete spectrum must be constructed and used. For example, at high $p_\perp$, where the trapping widths are relatively large, the number of waves in the discrete spectrum will only be ≈ 5 (and not ≈ 500).

A test-particle simulation intended to investigate transit-time acceleration for a given continuous spectrum and in the presence of pitch-angle scattering will then require the construction and use of many different discrete wave spectra. The discrete spectrum that will be used for a given particle in a given small time interval will depend on the value of $p_\perp$. This is a prohibitive task, and we will employ just the one discrete wave spectrum from case 2. We will then not be able to compare test-particle results with QLT, but we will be able to explore the dependence of the acceleration rate on the level of scattering.

We introduced pitch-angle scattering in the simulation by randomizing the pitch-angle cosine, μ, of each of the particles after a time, τ, has elapsed. Since particles can have negative $p_\parallel$ and still sometimes resonate, one could scatter over the interval $-1 \le \mu \le +1$; however, they would often be scattered into negative μ-space such that resonance with any wave is not possible (and computation is wasted on them). We tried adding 502 more waves, each with $k_\parallel < 0$ such that the entire 1004 wave spectrum was symmetric about $k_\parallel = 0$, to ensure that resonance would almost

always occur. The acceleration rate in this case was so huge (in qualitative agreement with QLT) that we could not determine whether we had employed small enough time steps (i.e., very different results were found when the time step was decreased, and this appeared to continue without limit). The validity of equations (2.4a) and (2.4b) is also in serious doubt. We instead opted for a rather artificial scenario, randomizing μ over the interval 0 to +1 (regardless of the initial value of μ) and staying with the 502 wave, case 2 spectrum. As in previous cases, 100 electrons were injected with initial $\tilde{p}_{\|}$ between 0.037 and 0.047 and with initial $\tilde{p}_{\perp} = 0.032$. Owing to the typically large number of resonant waves, a small time step was needed, and $0.025 T_{\rm H}$ was found to be sufficient.

Figure 8*a* shows the average dimensionless kinetic energy, $\tilde{E} = E/mc^2$, of the electrons for five different scattering times, τ. As $\tilde{\tau} = \tau/T_{\rm H}$ decreases from 100 to 6.25, the acceleration rate increases, reaches a maximum when $\tilde{\tau} = 12.5$, and then declines sharply. At $\tilde{t} = 2500$, the mean energy, $\langle \tilde{E} \rangle$, is greater than 1 in all five instances, as opposed to $\approx 5 \times 10^{-3}$ in the absence of scattering. Hence, energization is greatly enhanced with scattering.

We constructed a second discrete wave spectrum using the same parameters as in case 2 but with $\tilde{B}_i = 0.031$. This spectrum consisted of 637 waves and yielded a $W_{\rm B}(\eta)$ of the same shape as that in case 2 (see Fig. 1*a*) but with a total energy density, $\tilde{U}_{\rm B}$, about one-half as large and equal to 0.31. The $D_{\|\|}$ for $\tilde{p}_{\perp} = 0.032$ is about 1/2 times curve 1 in Figure 7*a*. The $D_{\|\|}$ at higher values of $\tilde{p}_{\perp}$ have similar shapes to those in Figure 7*a* but are not just one-half as large (remember that the spectrum was constructed with $\tilde{p}_{\perp} = 0.032$). The average particle energy resulting from this spectrum and the same values of τ is given in Figure 8*b*. As in Figure 8*a*, the acceleration rate is a maximum when $\tilde{\tau} = 12.5$. These two cases thus show the existence of an optimal scattering rate, at which energy gain is a maximum. Quasi-linear theory would predict that the energization rate be proportional to the wave energy density, $U_{\rm B}$, but this is not observed in these two cases as a result of our use of only one wave spectrum.

To illustrate the effect of $\tilde{k}_0$ on the optimal scattering rate, we built a third wave spectrum using the same parameters as in case 2 but with $\tilde{k}_0 = 2.5$ as opposed to 5. This spectrum has 502 waves and yields a $W_{\rm B}(\eta)$ that is the same as that in case 2 (see Fig. 1*a*). We show the average energy for the same five values of τ in Figure 8*c*. In this instance, the acceleration rate is a maximum when $\tilde{\tau} = 25$.

4. DISCUSSION

Cases 1–3 in § 3 demonstrate that there is excellent agreement between the predictions of QLT and the results of test-particle simulations in the absence of pitch-angle scattering. Quasi-linear theory is expected to break down eventually for strong turbulence, but these cases also illustrate that it is valid for $U_{\rm B}$ less than at least $\approx U_0$. Since the parallel diffusion coefficient, $D_{\|\|}$, determines the momentum diffusion coefficient, $D(p)$, when pitch-angle scattering keeps the distribution isotropic (see MLM), we can conclude that $D(p)$ is valid as well (but see below).

The test-particle simulations in case 4 illustrate an important point concerning transit-time acceleration in the presence of pitch-angle scattering: there is an optimal scattering timescale, at which the acceleration rate is a maximum. From the discussion in § 1, a particle gains or losses energy when it collides with a stationary perturbation (in the wave frame) and is reflected through conservation of the first adiabatic invariant. Pitch-angle scattering that occurs on a timescale shorter than the time it takes to reflect will redistribute a particle's pitch angle while it is interacting with a wave, break the first adiabatic invariant for the process, often cause the particle to pass through the perturbation instead of reflecting (since the particle begins interacting with the wave when its pitch angle is $\approx 90°$ and will very likely be scattered into smaller angles), and will inhibit energy gain over long timescales. The reflection lengthscale should be about the length of a compression, which is one-half the parallel wavelength, $\lambda_{\|}$. The reflection timescale, τ_r, is then $\lambda_{\|}/2v_{\|}$, which is equal to $\pi/kv_{\rm A}$ using the resonance condition.

Pitch-angle scattering that occurs on timescales greater than τ_r would transfer parallel energy into the perpendicular direction (on average) after several collisions, leading to acceleration that is more rapid than if there were no scattering and the magnetic moment remained constant. Pitch-angle scattering on a reflection timescale would cause this transfer to occur just after one collision and just before the next one, and it would maximize the magnetic moment (on average) for every collision. The last case would clearly maximize the energy gain rate. Hence, as the scattering rate increases from zero, the acceleration rate should increase, peak when $\tau \approx \tau_r$, and then decrease, independent of the value of B_i or $U_{\rm B}$. This is consistent with case 4. In particular, when $\tilde{k}_0 = 5$ (Figs. 8*a* and 8*b*), the acceleration rate is a maximum for $\tilde{\tau} = 12.5$, which is close to $\tilde{\tau}_r = 17$; when $\tilde{k}_0 = 2.5$ (Fig. 8*c*), the acceleration rate is a maximum when $\tilde{\tau} = 25$, which is about $\tilde{\tau}_r = 33$. Interestingly, the existence of an optimal scattering rate is contained in the work of Kulsrud & Ferrari (1971). The first term in their equation (7) gives the transit-time acceleration efficiency (see Melrose 1980, p. 73, since they referred to the unknown process as "collisional magnetic pumping in inhomogeneous fields"), and it is maximized when the ancillary scattering rate is $\approx kv_{\rm A}/3$. From above, our optimal rate is $kv_{\rm A}/\pi$, which is in excellent agreement with their analytical result.

The isotropic momentum diffusion coefficient, $D(p)$, is a μ average over $D_{\rm pp} = \mu^2 D_{\|\|}$ (e.g., MLM). While $D(p)$ should therefore be valid for a description of isotropic particle distributions (kept so by pitch-angle scattering), the question that now arises is the timescale over which the particle distribution is isotropized. There are two relevant timescales: the reflection timescale, which depends on k and is therefore not unique for a spectrum of waves in k-space, and the momentum change timescale, $\tau_p = p^2/D_{\rm pp}$ (e.g., Fisk 1976), which is usually much larger and depends on the amplitude and the *mean* wavenumber of the turbulence. The scattering timescale at which $D(p)$ is correct should be between these two limits. Because of the difficulty of performing a test-particle simulation with isotropizing scattering, this issue is best settled by comparing the results from the isotropic momentum diffusion equation in p-space with those from the full diffusion equation in p- and μ-space. This will be considered in the future, but we assume for the purposes below that scattering must occur on the shortest timescale (viz., τ_r).

Our test-particle results are at odds with those of Zweibel & de La Beaujardière (1990). In the absence of pitch-angle scattering, they found that the mean particle energy was only several times the thermal energy at ≈ 10 s, even for

$U_B > U_0$. With scattering, the energy gains were also very small. In either case, energization was not nearly rapid enough to account for flare electron acceleration. These low energies could be caused by using waves with small values of k (the details of the wave spectrum are not given), but they are more likely because of resonance gaps in their discrete spectra (see § 2.3). Hence, it appears that transit-time acceleration is fundamentally and severely limited in this case, but it is not so when continuous spectra are assumed for the flare acceleration region.

While pitch-angle scattering can greatly enhance the energization rate, we now consider whether it is indeed necessary in order for acceleration to occur under solar flare conditions. In order for electrons to be accelerated, two conditions must be met: (1) the systematic rate of energy gain, $\langle dE/dt \rangle_t$, resulting from transit-time interactions must be positive, and (2) if $\langle dE/dt \rangle_t$ is positive, it must be greater than the absolute value of the energy loss rate, $\langle dE/dt \rangle_c$, resulting from electron-electron Coulomb collisions.

Being a stochastic process, the change in particle energy over small times resulting from transit-time interactions has both systematic and diffusive components. This is also evident from the fact that equation (3.1) can be written as a Fokker-Planck equation in kinetic energy, E, space,

$$\frac{\partial N}{\partial t} = -\frac{\partial}{\partial E}\left(\left\langle \frac{dE}{dt} \right\rangle_t N\right) + \frac{1}{2}\frac{\partial^2}{\partial E^2}(DN), \qquad (4.1)$$

where $p_\perp$ is a constant, $D = 2D_{\parallel\parallel} v_\parallel^2$ is the energy diffusion coefficient $\langle (\Delta E)^2 \rangle / 2\,\Delta t$, and $\langle dE/dt \rangle_t = \partial(D_{\parallel\parallel} v_\parallel)/\partial p_\parallel$ is the systematic rate of energy gain. The quantity N is either the energy distribution, such that $\int_0^\infty dEN$ is the total number density of particles, or the single-particle probability density, such that dEN is the probability of the particle being in the interval dE about E. These equations are relativistically correct.

In a sufficiently small time interval, Δt, a delta function located at E_0 will spread into approximately a Gaussian shape, with a mean of $E_0 + \langle dE/dt \rangle_t \Delta t$ and a variance of $2D\,\Delta t$. Interpreting N as a probability density, a positive $\langle dE/dt \rangle_t$ means that the particle will probably gain energy in that time interval, which is the usual meaning of acceleration. For many of the transit-time $D_{\parallel\parallel}$, $\langle dE/dt \rangle_t$ is positive from $v_\parallel = v_A$ to a few times v_A and negative at larger $v_\parallel$. Does this mean that particles never reach these higher energies? No, solutions of equation (3.1) for all of the $D_{\parallel\parallel}$ considered show that the particle (or probability) flux in momentum space, $-D_{\parallel\parallel}\partial f/\partial p_\parallel$, is always positive, even in regions where $\langle dE/dt \rangle_t$ is negative. Physically, this results from diffusion, which ensures that there will be some particles that have gained energy in a time interval. In addition, since the total rate of energy gain of a distribution of particles, dU_p/dt, is $\int_0^\infty dEN\langle dE/dt \rangle_t$, $\langle dE/dt \rangle_t$ need not be positive everywhere for there to be a net flow of energy from the waves to the particles. The same solutions reveal that dU_p/dt is indeed always positive.

While particles can move to higher energies if $\langle dE/dt \rangle_t < 0$, the rate at which they do so is much less than if $\langle dE/dt \rangle_t > 0$. In those cases where $\langle dE/dt \rangle_t$ is negative above a few times the Alfvén speed, particles will not be pushed strongly to higher energies. In this case, wave energy will be deposited in those electrons at energies where $\langle dE/dt \rangle_t$ is positive, diffused to higher energies, and also redistributed by collisions. Particle heating (or something close to it) will be the result. In those cases where $\langle dE/dt \rangle_t$ is positive everywhere, there will be acceleration if $\langle dE/dt \rangle_t$ dominates the Coulomb energy loss rate. If it does not, particle heating will be the result again.

For a power-law spectral density, $\tilde{W}_B(\eta) = \tilde{W}_0 |\eta|^{-a}$, we find using equation (2.8) that

$$\left\langle \frac{d\tilde{E}}{d\tilde{t}} \right\rangle_t = \frac{\pi}{4}\tilde{v}_A^{2-a}\langle \tilde{k} \rangle \tilde{W}_0 \tilde{p}_\perp^4 |\tilde{p}_\parallel|^{a-3} \times [(a-2) - (a-4)\tilde{v}_A^2 \tilde{p}_\parallel^{-2}] \qquad (4.2)$$

for nonrelativistic energies and $a \neq +1$. When $a \leq 0$, $\tilde{W}_0 = (1+a)\tilde{U}_B/2$. When $a > 0$, the spectral density extends down to $|\eta| = \tilde{v}_A$ and $\tilde{W}_0 = (a-1)\tilde{U}_B[2(\tilde{v}_A^{1-a} - 1)]^{-1}$.

For a spectral density that peaks parallel and antiparallel to $\boldsymbol{B}_0$ ($a < 0$), the particles encounter a decreasing level of turbulence as they gain energy, and $\langle dE/dt \rangle_t$ is positive only for $v_A \leq v_\parallel < v_A[(4+a)/(2+a)]^{1/2}$. At higher $v_\parallel$, $\langle dE/dt \rangle_t$ is negative. Therefore, acceleration is confined to only a narrow range of supra-Alfvénic energies, and these spectral densities will produce electron heating. An isotropic spectral density ($a = 0$) has $\langle dE/dt \rangle_t$ positive for $v_A \leq v_\parallel < 2^{1/2} v_A$ and negative otherwise. Again, acceleration is confined to only a narrow range. For spectral densities peaked normal to the magnetic field, the electrons encounter a higher level of waves as they gain energy. If $0 < a < +2$, $\langle dE/dt \rangle_t$ is similar to that for $a = 0$. In both instances, the electrons will suffer heating instead of acceleration over a large energy range.

If the spectral density is more strongly peaked ($a \geq 2$) normal to the magnetic field, the transit-time energy gain rate is always positive and must next be compared with that for Coulomb collisions. We show $\langle dE/dt \rangle_t$ in Figure 9 for $a = 0$, 2, 3, and 4, along with $\langle dE/dt \rangle_c$ resulting from electron-electron Coulomb collisions (Huba 1994). We assumed a flare plasma in which the electron density, temperature, and magnetic field are 10^{10} cm^{-3}, 3×10^6 K, and 500 G, respectively. The turbulence was assumed to have $\langle \tilde{k} \rangle = 1$ and $\tilde{U}_B = 1$. We also used a $\tilde{p}_\perp$ equal to the thermal value of 0.032 in calculating $\langle dE/dt \rangle_t$. (The $\langle dE/dt \rangle_t$ curves do not extend below $\tilde{E} = \tilde{p}_\perp^2/2$, as this is the minimum energy an electron can have.) Below the thermal energy of $5 \times 10^{-4} mc^2$, $\langle dE/dt \rangle_c$ is positive, while above the thermal energy it is negative, and the electrons systematically lose energy.

For $a = 2$, electrons can be accelerated up to about 10 keV, at which point Coulomb losses dominate transit-time energy gain. For $a = 3$, acceleration can proceed up to arbitrarily high energies. For $a = 4$, the threshold for acceleration is more than 10 e-folding energies out in the tail of the thermal distribution, so that a negligible number of electrons will be accelerated (albeit to arbitrarily high energies) in this case. However, for smaller wave energy densities on the order of $10^{-3} U_0$ and mean wavenumbers well inside the MHD regime (such as in MLM), any positive portion of $\langle dE/dt \rangle_t$ will fall below the Coulomb energy loss rate. The result in this case will be heating, with Coulomb collisions distributing energy as rapidly as transit-time acceleration gives it to the electrons.

Hence, weak MHD fast mode turbulence will always produce electron heating under solar flare conditions in the absence of pitch-angle scattering. While significant electron heating does occur during impulsive flares (see, e.g., Lin &

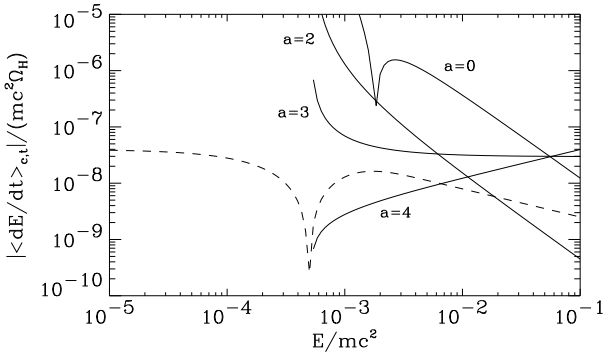

FIG. 9.—Systematic energy gain rates for transit-time interactions (*solid lines*) and for electron-electron Coulomb collisions (*dashed line*). Coulomb $\langle dE/dt\rangle$ is positive below the thermal energy of $\approx 5 \times 10^{-4}$ and negative above. For $a = 0$, $\langle dE/dt\rangle_t$ is positive below $\tilde{E} \approx 2 \times 10^{-3}$ and negative above. For the other values of a, $\langle dE/dt\rangle$ is positive.

Johns 1993), this process cannot account for acceleration and nonthermal power-law electron distributions up to ~ 100 keV. One immediate source of scattering is Coulomb collisions. For the plasma described in Figure 9, the Coulomb pitch-angle scattering timescale, τ_c, is $\approx 6 \times 10^{-3}$ s at the threshold energy. In order for τ_c to be approximately equal to the optimal pitch-angle scattering timescale, $\tilde{k}$ for the waves needs to be $\approx 3 \times 10^{-3}$. At 80 keV, $\tau_c \approx 8$ s, and $\tilde{k}$ must now be $\approx 2 \times 10^{-6}$. These values of k are quite low. Even if the electrons are isotropic from the Coulomb scattering and all the wave energy is concentrated at the optimal wavenumber, the energization rates $\langle d\tilde{E}/d\tilde{t}\rangle$ at the threshold energy and 80 keV (calculated from MLM) are $\approx 10^{-10}\tilde{U}_B$ and $\approx 4 \times 10^{-9}\tilde{U}_B$, respectively. For weak turbulence, these rates lie below the Coulomb energy loss rate (see Fig. 9). In reality, there will likely be a spectrum of waves. While the waves at higher k will energize the electrons faster in the parallel direction, Coulomb collisions will not scatter the electrons at the optimum rate for these waves. It thus appears that Coulomb collisions will not be the source of pitch-angle scattering that leads to acceleration but will likely increase the efficiency of heating (perhaps significantly). This will be investigated further in a future work (Lenters & Miller 1998).

Other sources of pitch-angle scattering are high-frequency plasma waves such as whistlers and lower hybrid waves, which can gyroresonate with the electrons. Contrary to early works (e.g., Melrose 1980, pp. 74–76; Achterberg 1981) that put the threshold for resonance with whistlers at ~ 100 keV, whistlers can gyroresonate with electrons above ~ 1 keV (Miller & Steinacker 1992), which is close to the threshold energy of $mv^2_A/2 \approx 0.3$ keV for transit-time acceleration. Whistlers can thus provide pitch-angle scattering soon after the electrons start gaining energy from the fast mode waves. They are highly efficient at scattering as well. For instance, the whistler pitch-angle scattering timescale, $\tilde{\tau}_w$, for a ≈ 2 keV electron is $\sim 6 \times 10^{-5}\tilde{U}_w$ in the plasma discussed above, where $\tilde{U}_w$ is the normalized whistler energy density, and we assumed that the whistlers had a $-5/3$ power-law spectral density (from Steinacker & Miller 1992). Hence, τ_w is about the optimal scattering timescale for fast mode waves with $\tilde{k} \sim 1$ if $U_w \sim 10^{-6}U_0$. This is an extremely low level of whistlers ($\sim 10^{-3}$ of the thermal particle energy density) and is much less than that needed for the whistlers to do the acceleration as well (Steinacker & Miller 1992). While there is still the chicken-and-egg problem mentioned in § 1, these levels are so low that it is not unreasonable to assume they will exist (possibly as a result of nonlinear wave-wave processes at lower k).

It has been suggested by Melrose (1980, p. 75) that anisotropies that develop in the electron distribution during collisions with the magnetic perturbations will generate whistlers. In this case, an external source is not needed, and the scattering waves are created self-consistently. The argument, however, is semiquantitative and addresses only those electrons with energies much above the transit-time threshold. Further work is need to establish this process. Another possibility is that waves are generated as a result of the anisotropic distribution that arises from the fast mode waves. Specifically, the fast mode waves will create an electron distribution with an excess of parallel energy (at least until it relaxes via Coulomb collisions), and this may at some point excite an instability that causes it to relax. In this instance, an external source of scattering waves is also not needed.

5. SUMMARY

We considered the interaction of electrons with a spectrum of fast mode waves using both test-particle simulations and QLT. Our specific results are as follows:

1. As far as moments of the electron distribution are concerned, QLT provides an excellent description of transit-time acceleration, even when the total energy density of the fast mode wave turbulence is about equal to the ambient magnetic field energy density.
2. When constructing a discrete wave spectrum that is to mimic a continuous one, the individual monochromatic waves must be placed (in angle and/or wavenumber) so that neighboring waves have overlapping resonances and the spectral density that results from binning the discrete waves matches the continuous one.
3. Pitch-angle scattering greatly increases the energization rate from transit-time acceleration. The energy gain rate from waves at a certain wavenumber, k, is a maximum when the pitch-angle scattering timescale is about equal to the time required for a particle to reflect from a wave compression, which is $\approx \pi/kv_A$. High-k waves thus require more rapid pitch-angle scattering for their acceleration rate to be maximal. Equivalently, electrons with a given scattering rate in the presence of a spectrum of waves in k-space will be accelerated by only a small fraction of the waves (at most) at their maximum rate.
4. Weak, fast mode wave turbulence in the absence of pitch-angle scattering will lead to electron heating under solar flare conditions. Pitch-angle scattering from Coulomb collisions is not sufficiently rapid to lead to electron acceleration but may significantly increase the heating rate. Whistler turbulence with an energy density of $\approx 0.1\%$ of the thermal energy density or of $\approx 10^{-4}\%$ of the ambient magnetic field energy density would be, for example, an agent that would scatter the electrons rapidly enough for acceleration to occur.

I thank Hui Li, Ted LaRosa, and Ron Moore for helpful discussions and the referee, Ellen Zweibel, for insightful comments. Support was provided by NASA Solar Physics Program grant NAGW–5082.

APPENDIX

TRAPPING WIDTH AND BOUNCE FREQUENCY

Suppose the ambient magnetic field is $B_0 \hat{z}$. Consider an oblique fast mode wave with propagation angle cosine η, magnetic field amplitude δB, and wavenumber k. The magnetic field amplitude and wavenumber along $\hat{z}$ are then $\delta B_\parallel = (1 - \eta^2)^{1/2} \delta B$ and $k_\parallel = \eta k$, respectively. We assume a nonrelativistic particle and a wave-parallel phase speed $\omega/k_\parallel \ll c$; wave frame quantities are denoted by a prime as in the text. Taking a rarefaction minimum to be at $z' = 0$, the parallel wave magnetic field, $B'_\parallel$, is then $-\delta B_\parallel \cos(k_\parallel z')$. Particle motion is governed by the magnetic mirror force, so that

$$m \frac{d^2 z'}{dt^2} = - \frac{m v_\perp^2}{2[B_0 - \delta B_\parallel \cos(k_\parallel z')]} k_\parallel \delta B_\parallel \sin(k_\parallel z') . \tag{A1}$$

If the particle is trapped between two compressions and makes small excursions from the rarefaction minimum and $\delta B \ll B_0$, equation (A1) becomes $d^2 z'/dt^2 = -\omega^2{}_b z'$, where

$$\omega_b^2 = \frac{v_\perp^2}{2} k_\parallel^2 \frac{\delta B_\parallel}{B_0} . \tag{A2}$$

Motion in the rarefaction minimum is therefore approximately simple harmonic with frequency ω_b.

The largest $v'_\parallel = dz'/dt$ a particle can have and still remain trapped between two compressions is called the trapping width, $\Delta v'_\parallel$, and is obtained by letting $v'_\parallel = \Delta v'_\parallel$ at the rarefaction minimum and $v'_\parallel = 0$ at the next compression maximum. For small amplitude waves, we then have from equation (A1) that

$$\int_{\Delta v_\parallel'}^{0} v'_\parallel \, dv'_\parallel = - \frac{v_\perp^2}{2} k_\parallel \frac{\delta B_\parallel}{B_0} \int_0^{\pi/k_\parallel} \sin(k_\parallel z') dz' , \tag{A3}$$

which yields

$$(\Delta v'_\parallel)^2 = 2 v_\perp^2 \frac{\delta B_\parallel}{B_0} . \tag{A4}$$

The trapping width in the wave frame is that same as in the plasma frame, $\Delta v_\parallel$.

The condition for trapping or resonance in the wave frame is then $v'_\parallel < \Delta v'_\parallel$, which in the plasma frame becomes $|v_\parallel - \omega/k_\parallel| < \Delta v_\parallel$. With equations (A2) and (A4), the resonance condition in the plasma frame can also be written in terms of the frequency mismatch as $|\omega - k_\parallel v_\parallel| < 2\omega_b$.

REFERENCES

Achterberg, A. 1979, A&A, 76, 276
———. 1981, A&A, 97, 259
de La Beaujardière, J.-F., & Zweibel, E. G. 1989, ApJ, 336, 1059
Dennis, B. R. 1985, Sol. Phys., 100, 465
Eichler, D. 1979, ApJ, 229, 409
Fermi, E. 1949, Phys. Rev., 75, 1169
Fisk, L. A. 1976, J. Geophys. Res., 81, 4633
Forbes, T. G. 1996, in High-Energy Solar Physics, ed. R. Ramaty, N. Mandzhavidze, & X.-M. Hua (New York: AIP), 275
Gary, S. P. 1993, Theory of Space Plasma Microinstabilities (Cambridge: Cambridge Univ. Press)
Ginet, G. P., & Heinemann, M. A. 1990, Phys. Fluids B, 2, 701
Gisler, G. 1992, in Particle Acceleration in Cosmic Plasmas, ed. G. P. Zank & T. K. Gaisser (New York: AIP), 229
Gisler, G., & Lemons, D. 1990, J. Geophys. Res., 95, 14925
Hamilton, R. J., & Petrosian, V. 1992, ApJ, 398, 350
Huba, J. D. 1994, NRL Plasma Formulary (NRL/PU/6790–94–265) (Washington, DC: Naval Research Laboratory),
Karimabadi, H., Akimoto, K., Omidi, N., & Menyuk, C. R. 1990, Phys. Fluids B, 2, 606
Karimabadi, H., Krauss-Varban, D., & Terasawa, T. 1992, J. Geophys. Res., 97, 13853
Karimabadi, H., & Menyuk, C. R. 1991, J. Geophys. Res., 96, 9669
Kiplinger, A. L., Dennis, B. R., Emslie, A. G., Frost, K. J., & Orwig, L. E. 1983, ApJ, 265, L99
Kulsrud, R. M., & Ferrari, A. 1971, Ap&SS, 12, 302
Landau, L. D., & Lifshitz, E. M. 1962, The Classical Theory of Fields, trans. M. Hamermesh (Reading, MA: Addison-Wesley), 37–38
LaRosa, T. N., & Moore, R. L. 1993, ApJ, 418, 912
LaRosa, T. N., Moore, R. L., Miller, J. A., & Shore, S. N. 1996, ApJ, 467, 454
LaRosa, T. N., Moore, R. L., & Shore, S. N. 1994, ApJ, 425, 856
Lenters, G. T., & Miller, J. A. 1998, ApJ, in press
Lichtenberg, A. J., & Lieberman, M. A. 1983, Regular and Stochastic Motion (New York: Springer), 28
Lin, R. P., & Johns, C. M. 1993, ApJ, 417, L53
Lin, R. P., & Schwartz, R. A. 1987, ApJ, 312, 462
Machado, M. E., Ong, K. K., Emslie, A. G., Fishman, G. J., Meegan, C., Wilson, R., & Paciesas, W. S. 1993, Adv. Space Res., 13(9), 175
Melrose, D. B. 1980, Plasma Astrophysics, Vol. 2 (New York: Gordon & Breach)
Miller, J. A., et al. 1997, J. Geophys. Res., 102, 14631
Miller, J. A., LaRosa, T. N., & Moore, R. L. 1996, ApJ, 461, 445 (MLM)
Miller, J. A., & Ramaty, R. 1987, Sol. Phys., 113, 195
Miller, J. A., & Steinacker, J. 1992, ApJ, 399, 284
Reames, D. V., Meyer, J. P., & von Rosenvinge, T. T. 1994, ApJS, 90, 649
Roberts, D. A., Goldstein, M. L., Matthaeus, W. H., & Ghosh, S. 1992, J. Geophys. Res., 97, 17115
Steinacker, J., & Miller, J. A. 1992, ApJ, 393, 764
Stix, T. H. 1992, Waves in Plasmas (New York: AIP), 273–292
Zweibel, E. G., & de La Beaujardière, J.-F. 1990, Geophys. Res. Lett., 17, 2051